Available online at www.sciencedirect.com
ScienceDirect
Journal of Magnetic Resonance 192 (2008) 131–138
JMR Journal of Magnetic Resonance
www.elsevier.com/locate/jmr

A simple, small and low cost permanent magnet design to produce homogeneous magnetic fields

B. Manz *, M. Benecke, F. Volke

Arbeitsgruppe Magnetische Resonanz, Fraunhofer-Institut für Biomedizinische Technik, Ensheimer Straße 48, 66386 St. Ingbert, Germany

Received 10 January 2008; revised 7 February 2008
Available online 15 February 2008

Abstract

A new portable, pocket-size NMR probe based on a novel permanent magnet arrangement is presented. It is based on a Halbach-type magnet design which mimics the field of a spherical dipole by using cylindrical bar and ring magnets. The magnet system is made up of only three individual magnets, and most field calculations and optimisations can be performed analytically. A prototype system has been built using a set of small, off the shelf commercially available permanent magnets. Proton linewidths of 50 ppm FWHM could be achieved at a field strength of 1 T. Calculations show that with custom-sized permanent magnets, linewidths of less than 1 ppm can be achieved over sample volumes of up to 1 mm^3, which would in theory enable chemical shift resolved proton spectroscopy on mass-limited samples. But even with the achieved linewidth of 50 ppm, this can be a useful portable sensor for small amounts of liquid samples with restricted molecular mobility, like gels, polymers or high viscosity liquids.

Keywords: Portable NMR; Permanent magnets; Table-top NMR; Halbach array

1. Introduction

In recent years, there has been considerable progress in the development of portable NMR devices. Starting from inside-out probes for borehole applications [1,2], a variety of more sophisticated portable NMR probes has been built since. Based on the magnet design and the application, these sensors can be categorised into two groups: The first group operates with open, or one-sided access, magnet systems and is usually applied to large samples, which are too large or too immobile to be transported to a laboratory magnet [3–14]. Although such NMR sensors are now routinely used for applications such as relaxation time analysis (e.g. mechanical properties of polymers, water/fat content of dairy products) [15–19], profiling [6,7,10,14] and flow measurements [20,21], due to magnetic field inhomogeneity they fail with the acquisition of high resolution NMR spectra, unless special techniques are applied [22–25]. The second group is based on small, closed magnet systems producing a homogeneous magnetic field at the sample location. One way to create homogeneous magnetic fields in these so-called table-top devices is to use a Halbach-type [26] array of permanent magnets. The idea is that the field of multipole magnets can be mimicked by an arrangement of individual magnet segments which are placed on a cylindrical shell and polarised in the direction of the field lines created by this magnetic multipole inside the cylinder. For example, for high resolution NMR spectroscopy, homogeneous flux inside a volume containing the sample is required, which can be produced by a dipolar Halbach array [27–30]. In order to reach the required homogeneity, these arrays usually consist of tens of individual magnet elements, each of which has to be positioned and held in place requiring a costly and tedious process [28].

Currently existing permanent magnet systems based on the Halbach design are able to achieve field homogeneities of approximately 30 ppm over a sample volume of 60 mm^3 [27], which is insufficient for chemical shift resolved proton spectroscopy. However, it is hoped that further improve-

* Corresponding author. Fax: +49 6894 980400.
E-mail address: bertram.manz@ibmt.fraunhofer.de (B. Manz).

1090-7807/$ - see front matter © 2008 Elsevier Inc. All rights reserved.
doi:10.1016/j.jmr.2008.02.011

ment will enable the on-site analysis of mass-limited samples, e.g. small quantities of potentially hazardous chemicals or drugs, in the near future. For example, the spectral linewidth can easily be reduced by decreasing the sample size in the saddle region of the magnetic field. The use of NMR microcoils may not only lead to enhanced spectral resolution, but also to increased sensitivity for mass-limited samples. The achievable size and filling factor of solenoidal microcoils is currently mainly limited by the manual fabrication process using thin wire, which leads to a detection limit of a few picolitres [31]. With novel fabrication techniques using laser-lathe lithography [32] complex three-dimensionally shaped microcoils can be produced, leading to a further reduction of the detection limit.

Another method to enhance spectral resolution is to improve the quality of the magnetic field itself. This can be achieved by adding more elements to the Halbach array, as demonstrated by Raich and Blümler [28]. Zhang et al. have suggested a three-dimensional arrangement, where the individual bar magnets are placed in two orthogonal layers of a Halbach-type structure [30]. Their calculations showed that the field profiles can be improved significantly with this design.

In this contribution we will describe a magnet system, which mimics the field of a spherical dipole similar to the one suggested by Zhang et al., but retaining a spherical symmetry by using cylindrical bar and ring magnets [33]. Since only a small number of magnets is used, the probe is easy to assemble. We will show that with such a small and simple setup highly homogeneous magnetic fields can be generated.

2. Magnet design

Fig. 1a shows schematically the magnetisation of a dipolar Halbach array [28]. Its flux is homogeneous inside and perfectly shielded outside the cylinder shell. The most simple discrete element representation consists of four identical bar magnets (Fig. 1b) and has been demonstrated by Hills et al. [29]. Our suggested design shown in Fig. 1c is a spherical extension of this four element arrangement using cylindrical bar magnets and a ring magnet along the equatorial plane. Since the cylindrical geometry of the

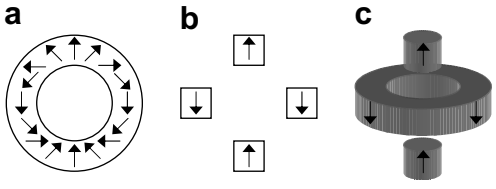

Fig. 1. (a) A schematic drawing of the magnetisation in a dipolar Halbach array. (b) The most simple practical implementation of the dipolar Halbach array using four identical bar magnets. (c) A spherical Halbach-type arrangement can be obtained through rotation of the structure shown in (b) around the vertical axis.

original Halbach design is no longer maintained, and the magnet elements are no longer equal in shape and size, the magnetic field cannot be expected to be homogeneous in the centre. However, we will show that by making some adjustments to the magnet dimensions and separations, this field homogeneity can be regained.

In a first step we neglect the ring magnet and consider the magnetic field B_b of the bar magnets alone. Their length and radius should be denoted by l_b and r_b, respectively, and magnetised with a residual magnetisation B_r. Along the axis, the magnetic field strength can be calculated analytically, with the origin at the centre between the two bar magnets. Due to the cylindrical symmetry, both radial and angular components of B_b vanish, and the axial component $B_{b,z}$ is given by [34]:

$$B_{b,z} = \frac{B_r}{2}\left(\frac{z+l_b+d_b}{\sqrt{(z+l_b+d_b)^2+r_b^2}} - \frac{z+d_b}{\sqrt{(z+d_b)^2+r_b^2}} - \frac{z-l_b-d_b}{\sqrt{(z-l_b-d_b)^2+r_b^2}} + \frac{z-d_b}{\sqrt{(z-d_b)^2+r_b^2}}\right), \quad (1)$$

where $2d_b$ is the separation of these bar magnets.

The axial symmetry of the arrangement implies that all odd order derivatives vanish at the origin $z = 0$. Therefore, magnetic field homogeneity at the centre is governed by the second derivative of Eq. (1), which can easily be calculated:

$$B''_{b,z}(z=0) = -6r_b^2 B_\mathrm{r}\left(\frac{l_b+d_b}{((l_b+d_b)^2+r_b^2)^{5/2}} - \frac{d_b}{(d_b^2+r_b^2)^{5/2}}\right). \quad (2)$$

In Fig. 2a, the value of $B''_{b,z}(z=0)$ is shown as a function of d_b for several sets of bar magnets with different lengths and diameters. The highest homogeneity is achieved when $B''_{b,z}(z=0) = 0$. For a given set of bar magnets, the matching separation $d_{b,\mathrm{opt}}$ can be computed by finding the zero-crossing of Eq. (2), for example through the Newton–Raphson iteration [35].

The curves shown in Fig. 2a visualise the influence of the magnet geometry on the optimum magnet separation. For example, $d_{b,\mathrm{opt}}$ increases with decreasing bar magnet length and increasing bar magnet radius. In order to accommodate a small rf coil with sample and possibly a set of shim and/or gradient coils, the separation of the bar magnets should not be less than approximately 3 mm, which limits $d_{b,\mathrm{opt}}$ to values larger than 1.5 mm. This can be achieved by choosing the bar magnet size appropriately to guarantee that the zero-crossing of $B''_{b,z}(z=0)$ falls within the required range.

A more sophisticated way to shift the zero-crossing of $B''_{b,z}(z=0)$, which can lead to even higher magnetic field homogeneity, is to embed the bar magnet arrangement inside a ring magnet of outer diameter $2r_a$, inner diameter $2r_i$ and length $2l_r$, which leads to the Halbach-type setup

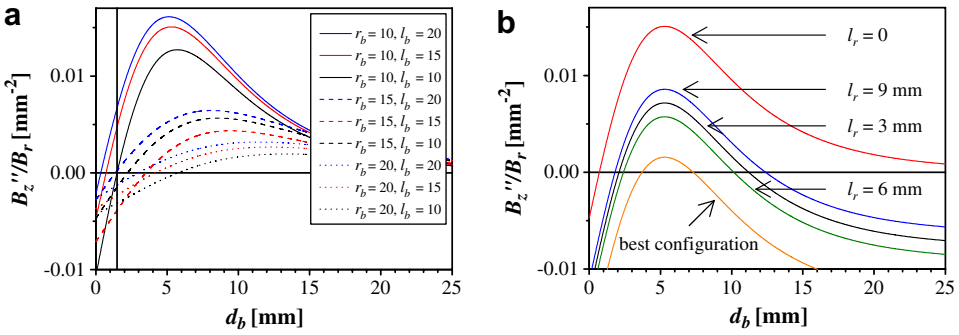

Fig. 2. (a) The second derivative of the magnetic field strength at the central point between two identical cylindrical bar magnets is shown as a function of gap size between these magnets. The individual curves correspond to magnets with different radii r_b and lengths l_b (in mm). The vertical line at $d_b = 1.5$ mm marks the minimum separation which is needed to accommodate a sample tube and rf coil. In (b) it is shown how a ring magnet affects the field homogeneity. Best field homogeneity is achieved for larger bar magnet separations than without a ring magnet. In this graph, a bar magnet radius of 10 mm and length of 15 mm was assumed. The ring magnet had an inner radius of 11.5 mm and an outer radius of 20 mm. The curve denoted as best configuration corresponds to a magnet setup where both the second and fourth derivatives of B_z vanish at the origin. See text for details.

shown in Fig. 1c. The axial component of the magnetic field $B_{r,z}$ purely from the ring magnet is given as:

$$B_{r,z} = \frac{B_r}{2}\left(\frac{z+l_r}{\sqrt{(z+l_r)^2+r_a^2}} - \frac{z-l_r}{\sqrt{(z-l_r)^2+r_a^2}} - \frac{z+l_r}{\sqrt{(z+l_r)^2+r_i^2}} + \frac{z-l_r}{\sqrt{(z-l_r)^2+r_i^2}}\right). \quad (3)$$

As with the bar magnets, the axial symmetry of the arrangement guarantees that all odd order derivatives vanish at the origin. A calculation of the second derivative of Eq. (3) yields:

$$B''_{r,z}(z=0) = -6 l_r B_r \left(\frac{r_i^2}{(l_r^2+r_i^2)^{5/2}} - \frac{r_a^2}{(l_r^2+r_a^2)^{5/2}}\right). \quad (4)$$

The total magnetic field strength $B_z(z)$ is then given as the sum of Eqs. (1) and (3). The effect of adding a ring magnet with given dimensions is to shift the curves shown in Fig. 2a down. This is shown in Fig. 2b for several ring magnets. As a consequence, two zero-crossings exist, out of which only the one with the smaller value of d_b shall be considered, since at this value the corresponding magnetic field strength is much higher. As required, and by simply using standard commercially available ring magnets, this zero-crossing can be moved to higher values of d_b compared to the arrangement with no ring magnet, adding space for the rf coil and possibly further equipment, without compromising in field strength and homogeneity. In the centre of the arrangement, the magnetic fields of the bar and ring magnet overlap constructively, with the ring magnet contributing typically 14–24% to the total magnetic field strength for ring magnet lengths between 6 and 18 mm. The resulting axial field homogeneity is shown in Fig. 3a. For the radial field profile of such a magnet arrangement a simple analytical solution does not exist. However, we note that in the case of cylindrical symmetry Maxwell's equations provide a simple relationship between axial and radial field homogeneity at the origin $(r,z) = (0,0)$:

$$\frac{\partial^2 B_z}{\partial r^2} + \frac{\partial^2 B_z}{\partial z^2} = 0. \quad (5)$$

Finite element (FEM) simulations using the 2D-freeware package FEMM 4.0 (D. Meeker, Foster-Miller Inc., Waltham, MA) were performed in order to calculate both axial and radial field profiles. The axial field profiles showed excellent agreement with the analytical calculations, and the resulting radial profiles of the FEM simulations are shown in Fig. 3b. The magnetic field is very homogeneous in the centre, consistent with the requirement $B_z''(z=0) = 0$. For r and z values smaller than 0.5 mm, the field homogeneity is better than 2 ppm, and therefore good enough to at least resolve water and hydrocarbon peaks with a splitting of approx. 3.5 ppm. However, it should be noted that mechanical tolerances in the magnet holder and magnets themselves, as well as inhomogeneous magnetisation of the individual magnets and temperature effects will lead to further line broadening in a real system.

By additionally allowing the geometry of the ring magnet to vary, it is even possible to find a solution where the first five derivatives of B_z vanish in the centre. Since there is one additional condition with $B_z^{(4)}(z=0) = 0$, but three extra independent parameters r_i, r_a and l_r, an infinite number of possible solutions exists. The magnetic field profile of one such solution ($r_b = 10$ mm, $l_b = 15$ mm, $r_i = 10$ mm, $r_a = 25$ mm, $l_r = 3.1$ mm, $d_b = 3.77$ mm) is shown in Fig. 3, where the field homogeneity is better than 1 ppm over r and z values smaller than up to 1 mm.

3. Setup of the magnet system

The goal of this study was to produce a small, inexpensive NMR magnet using off the shelf commercially available permanent magnets. All magnets were made of NdFeB with a residual magnetisation of $B_r = 1.2$ T and

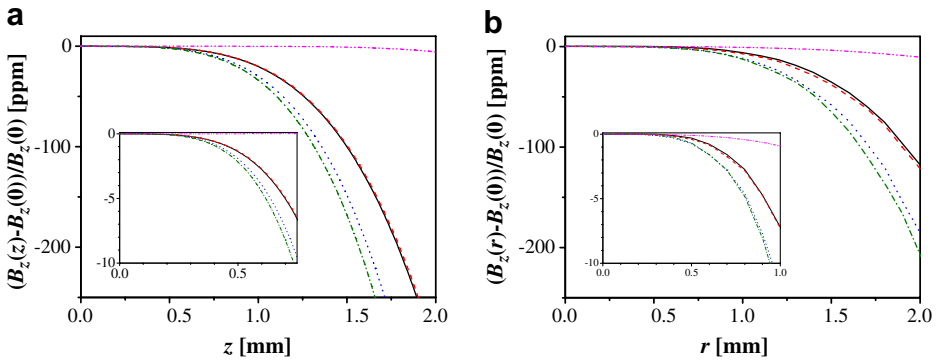

Fig. 3. The graphs show the calculated magnetic field strength along the axial (a) and radial (b) direction for a ring magnet with length $2l_r = 0$ (—), 6 mm (---), 12 mm (···), 18 mm (- · - ·). A bar magnet radius of 10 mm, length of 15 mm and separation for maximum homogeneity, as described in the text, was assumed. The curve (- · - ·) shows the magnetic field strength for a magnet configuration where both the second and fourth derivatives of B_z vanish at the origin. The inset displays an enlargement of the region with small z and r.

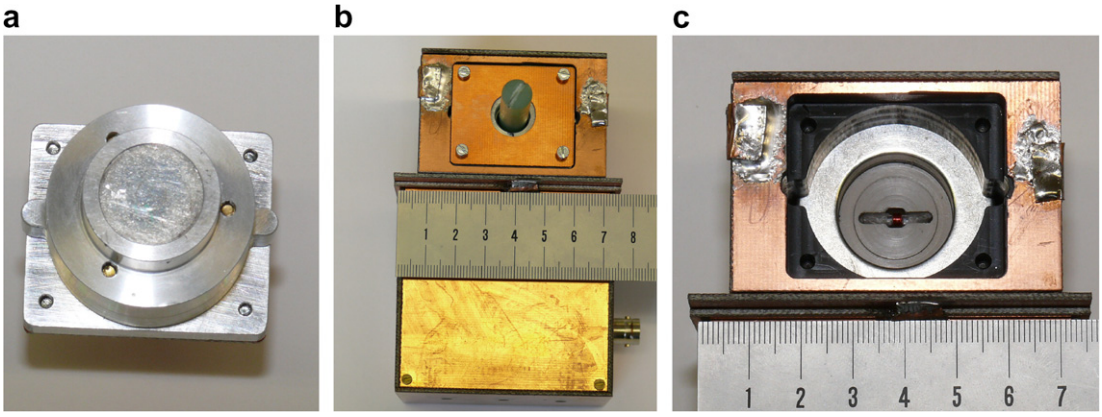

Fig. 4. Photographs of the probe. In (a) one of the bar magnets is shown inside its aluminium holder. The entire probe is shown in (b), with the shielded casing for the magnets (top) and the housing for the rf tuning capacitors (bottom, underneath the ruler). In (c) one of the bar magnets has been removed in order to show the ring magnet and the rf coil inside its holder.

were purchased from IBSMagnet (Berlin, Germany). Bar and disc magnets are available in a wide range of sizes. It was decided to use bar magnets with dimensions $r_b = 10$ mm, $l_b = 15$ mm, since calculations with these parameters yielded good results. These magnets were made by attaching two bar magnets of length 10 and 5 mm together. For ring magnets, the commercially available sizes are far more limited. A ring with $r_i = 11.5$ mm, $r_a = 20$ and 6 mm thickness was suitable for our needs. By stacking up to three ring magnets together, the ring length $2l_r$ could be varied in discrete steps from 0 to 18 mm. The bar magnets were positioned and firmly held in place by a specially designed aluminium case shown in Fig. 4a, which is equipped with a number of screws to permit axial movement with an accuracy of approximately 50 μm. The complete magnet system had to be placed inside a copper box for rf shielding. It has a size of $7 \times 6.5 \times 4.5\ \text{cm}^3$, weighs approximately 600 g and is shown in Fig. 4b.

A solenoid rf coil was wound around a 1.9 mm o.d. (1.5 mm i.d.) glass capillary filled with silicon oil (viscosity 0.3 Pa s), which had been purchased from a local pharmacy. The coil, as visible in Fig. 4c, consisted of 18 turns of 0.1 mm diameter insulated copper wire in two layers and had a length of 1.8 mm. In order to avoid crushing the coil and sample tube when adjusting the bar magnet separation, their minimum separation $2d_{b,\min}$ was mechanically limited to 2 mm.

Due to the location and size of the ring magnet it is impossible to measure the magnetic field strength inside the magnet system. We therefore needed to rely on the calculations in order to estimate the resonance frequency and field strength, which is around 1 T. Using three adjustable capacitors (5–30 pF) in a balanced matching network [36], the coil circuit was tuned to a resonance frequency 43 MHz with a tuning range of 38–68 MHz.

4. Experimental

All experiments were performed using the broadband X channel of a Bruker Avance 400 MHz spectrometer and Topspin 1.5 software (Bruker, Rheinstetten, Germany). Spectra were acquired with a spin–echo pulse sequence,

where the rf pulse durations were 1 μs and an interpulse spacing of 1 ms.

The magnet system was prepared with n ($n = 0$–3) ring magnets in order to vary the ring length $2l_r$. For each ring length $2l_r$ a series of spectra was recorded in the following way (cf. flow chart in Fig. 5). Initially, the separation of the bar magnets was set to its minimum value of 4 mm. Since the magnetic field strength and therefore the Larmor frequency were not known accurately, a series of broadband spectra (500 kHz bandwidth) was recorded at different carrier frequencies until the NMR signal was found and on resonance. Then the carrier frequency was decreased in steps of 500 kHz, whilst the axial position of the bar magnets was adjusted until the signal was on resonance again. In a kind of shimming procedure the adjustment screws were finely tuned for each frequency step in order to achieve a long echo decay and resulting narrow resonance line. On the average, the bar magnets had to be separated by approximately 0.2 mm in order to accommodate this frequency shift. We also noticed that turning the bar magnets around their axes had a dramatic effect on the signal decay. This is probably due to inhomogeneous magnetisation of the permanent magnets. Once all adjustments had been made, a spectrum was recorded using 8 signal averages.

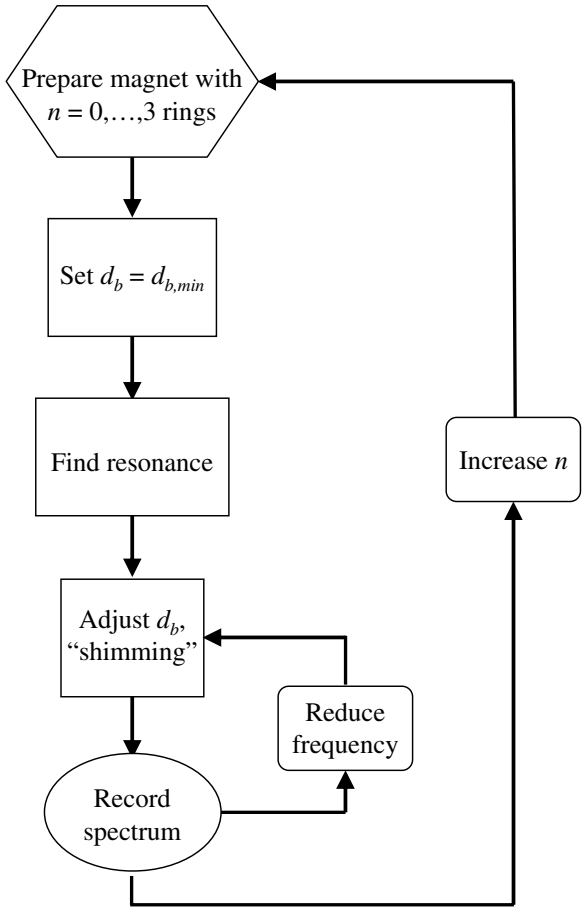

Fig. 5. Flow chart for finding the ^{1}H resonance and recording spectra at different magnet configurations. Details see text.

5. Results and discussion

A series of spectra recorded on the magnet system with 1 ring ($2l_r = 6$ mm) is shown in Fig. 6a. Initially, for $d_b = d_{b,\min}$, the resulting peak is very broad and non-symmetrical due to the inhomogeneous magnetic field. With increasing d_b, the line becomes narrower and symmetrical in shape, because we approach the zero-crossing of $B_z''(d_b, z = 0) = 0$ (cf. Fig. 2b). As d_b increases further through the cross-over at $d_b = d_{b,\text{opt}}$, the lines broaden again and lose their symmetry. The distortions in the spectral lines permit us to draw further conclusions about the shape of the magnetic field inside the sample volume. It can be seen that for $d_b > d_{b,\text{opt}}$ the tails of the spectra are leaning towards low field, which implies that the second derivative of the magnetic field must be negative. Since for the curves shown in Fig. 2b, the second z derivative of the field is positive for $d_b > d_{b,\text{opt}}$, these distortions in the line shape must due to Eq. (5) be caused by field inhomogeneities along the radial direction.

Fig. 6b shows the value of $d_{b,\text{opt}}$ as a function of l_r, both calculated from Eqs. (2) and (4) (line), as well as experimental values (symbols). The agreement between calculated and experimental values is very good, considering that there are no adjustable parameters involved in the calculation of $d_{b,\text{opt}}$.

The Larmor frequency ν_L of the NMR signal provides a simple method to measure the magnetic field strength B_0 at the sample location via the well-known relationship $\nu_L = \gamma B_0/2\pi$. In Fig. 6c the measured values of B_0 are displayed as symbols, both for bar magnet separations $d_b = d_{b,\min}$ and $d_b = d_{b,\text{opt}}$. The agreement with the calculated values is excellent for $B_r = 1.26$ T, which is very consistent with the manufacturer's specifications of $B_r = 1.2$ T.

Since the experimental and calculated values for field strength and optimisation parameters agree so well, we now consider the field profiles. For the sample size used here (length 1.8 mm, diameter 1.5 mm), a linewidth of below 10 ppm can be expected from the calculated field profiles shown in Fig. 3. However, the best spectrum recorded so far had a full base linewidth of 32 kHz (850 ppm) and a full linewidth at half maximum (FWHM) of 2 kHz (50 ppm), which is almost two orders of magnitude worse than theoretically possible, but comparable to signals measured using Halbach arrays [27,28]. Approximately 25% of the total signal was found within the 50 ppm FWHM range.

The symmetrical shape of this spectrum at the best field homogeneity suggests some odd order field variations. Because the position of the magnets can be adjusted very finely by a number of screws, and small adjustments are visible in the spectrum, we can almost certainly exclude mechanical tolerances to be the cause of this mismatch. We rather believe that it originates from slight inhomogeneities of the magnets themselves. Such inhomogeneities can either be due to inhomogeneous magnetisation in the manufacturing process or due to inhomogeneous tempera-

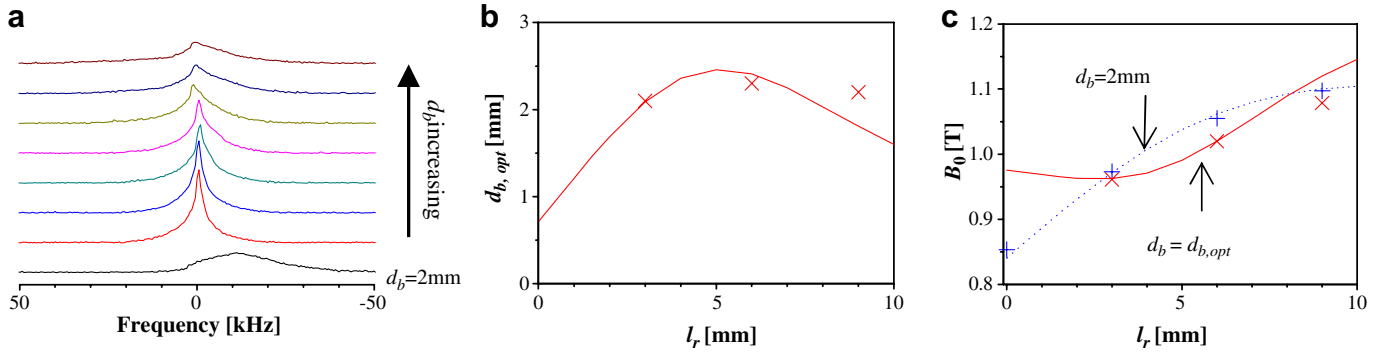

Fig. 6. (a) A series of spectra recorded on the magnet system with 1 ring ($2l_r = 6$ mm). With increasing bar magnet separation d_s, the resonance line first becomes narrower due to increased field homogeneity. After crossing the saddle point of $B_z''(d_b, z = 0) = 0$, the field homogeneity decreases again with increasing d_s, leading to broader resonance lines. The value of $d_{b,\mathrm{opt}}$ as a function of l_r is shown in (b), both calculated (—) from Eqs. (2) and (4), as well as experimental values (x). (c) The values of the magnetic field strength can be calculated from the measured Larmor frequency. These values are displayed as symbols, both for $d_b = d_{b,\mathrm{min}}$ (+) and $d_b = d_{b,\mathrm{opt}}$ (x) and compared to the magnet calculations (lines).

ture across the magnets. The large temperature drift of the Larmor frequency in magnets using NdFeB materials is well known. With a temperature coefficient of -1200 ppm/K [37], a temperature gradient of 0.1 K could lead to field inhomogeneities within the observed range. In order to clarify whether temperature gradients within the magnets are responsible for the observed mismatch between measured and calculated linewidth, the temperature inside the magnet box was measured, whilst simultaneously spectra were recorded every 10 min over 24 h. Due to the natural day/night temperature fluctuation in the laboratory, the total temperature change inside the magnet box was 2.2 °C. Although the total line shift was 2600 ppm over the experiment, no significant change in line shape could be observed. Even after storing the magnet box in a refrigerator over night and subsequently recording spectra during the equilibration process to room temperature, a line broadening could not be noticed. However, after assembling the magnet system by hand, an equilibration period of approximately 2 h was needed in order to obtain narrow lines. Therefore, thermal gradients can be excluded and we establish small inhomogeneities in magnetisation during the manufacturing process as the most likely cause for the observed line broadening.

6. Conclusions

In a recent paper it has been stated that "the sustainability of a portable NMR system for chemical analysis of samples in the field is within reach" [32]. Several companies (magritek, Tecmac, GE Security) have developed and now offer the required electronics for sale. Portable magnets with homogeneous fields are commercially available as well. Most of these systems concentrate on producing the required magnetic field homogeneity using Halbach designs. In this paper, we have suggested an alternative approach by conserving the rotational symmetry of a magnetic dipole. By using off the shelf commercially available permanent magnets, we were able to construct a pocket-size NMR sensor which reaches linewidths of 50 ppm FWHM at a field strength of 1 T. This is comparable to values achieved with much larger Halbach arrays. In our view, the beauty of the system described here lies in the simplicity of the magnet arrangement. Contrary to the Halbach design, where tens to hundreds of small permanent magnets need to be positioned and held in place requiring a costly and tedious process, our design merely requires a minimum of three magnets. Furthermore, magnetic field calculations can be performed analytically, which is a huge advantage when trying to optimise parameters.

One drawback of the presented design is clearly the accessibility to the sample. In the current prototype, one of the bar magnets has to be removed in order to change the sample. A trained user manages to re-assemble and tune the magnet system within a few minutes. Although such a procedure is comparable to shimming the field in a high resolution magnet, it is unacceptable with the requirements for a versatile mobile sensor. For future models, one could investigate how much field homogeneity is lost by drilling a small hole radially through the ring magnet in order to gain sample access. Alternatively, the ring magnet could be replaced by two rings with a small gap through which the sample can be inserted [33].

Using custom-built magnets, in theory a field homogeneity of less than 1 ppm can be achieved over sample volumes of 1 mm^3. A system made of real magnets is expected to be worse in performance by a factor of 10–100 for several reasons. NdFeB materials tend to be inhomogeneous in magnetisation, which is an additional source of line broadening. This can be reduced by scanning a large number of magnets with a Gaussmeter and choosing the best ones to be used in the magnet system. The range of accuracy for this section process is limited by the relative accuracy of the Gaussmeter, which is usually in the range of a few percentage. Smaller inhomogeneities and mismatches between the magnets can be accounted for by positioning the magnets in a way that these mismatches are compensated, for example by rotation and/or slight axial mismatch of the individual magnets. However, mechanical tolerances in the alignment of the magnets are unavoidable

and become more severe for small systems, since the fractional effects become larger. Reducing the magnet size significantly compared to the current design would decrease the sensitive volume, thus leading to a decrease in signal strength. Furthermore, then the size of the entire sensor would be dominated by the size of the surrounding components, like magnet holders, tuning capacitors etc. We therefore consider the current design a good compromise in terms of portability, mechanical manufacturing and achievable signal strength.

In the system described here, the separation of the bar magnets could be adjusted with an accuracy of approximately 50 μm. Even such fine adjustments had a visible, but not dramatic effect on the shape of the resulting spectrum. In order to be able to make adjustments of that size, the accuracy in the manufacturing process should be in the range of 10 μm, which is quite feasible using modern CAM engineering.

As spectral resolution is enhanced through the measures described above, the system will finally be susceptible to very fine temperature gradients and fluctuations. An efficient thermal insulation as well as a frequency lock will be mandatory to commercial high resolution portable NMR sensors. Finally, remaining field inhomogeneities will have to be compensated by a set of shim coils, as it is common practise for other high resolution NMR magnets. However, for many NMR applications, even proton linewidths of 50 ppm are sufficient for a quick characterisation of samples via relaxation and/or diffusion contrast, like gels, polymers or high viscosity liquids.

References

[1] J.A. Jackson, L.J. Burnett, J.F. Harmon, Remote(inside-out) NMR. III. Detection of nuclear magnetic resonance in a remotely produced region of homogeneous magnetic field, J. Magn. Reson. 41 (1980) 411–421.

[2] R.L. Kleinberg, A. Sezginer, D.D. Griffin, M. Fukuhara, Novel NMR apparatus for investigating an external sample, J. Magn. Reson. 97 (1992) 466–485.

[3] G. Eidmann, R. Savelsberg, P. Blümler, B. Blümich, The NMR MOUSE, a Mobile Universal Surface Explorer, J. Magn. Reson. A 122 (1996) 104–109.

[4] P. Prado, NMR hand-held moisture sensor, Magn. Reson. Imaging 19 (2001) 505–508.

[5] E. Fukushima, J.A. Jackson, Unilateral magnet having a remote uniform field region for nuclear magnetic resonance, US Patent No 6, 828, 892, 2004.

[6] J. Perlo, F. Casanova, B. Blümich, Profiles with microscopic resolution by single-sided NMR, J. Magn. Reson. 176 (2005) 64–70.

[7] S. Rahmatallah, Y. Li, H.C. Seton, I.S. Mackenzie, J.S. Gregory, R.M. Aspdena, NMR detection and one-dimensional imaging using the inhomogeneous magnetic field of a portable single-sided magnet, J. Magn. Reson. 173 (2005) 23–28.

[8] S. Utsuzawa, R. Kemmer, Y. Nakashima, K. Kose, Unilateral NMR apparatus using a novel barrel magnet, in: 46th Experimental NMR Conference, Providence, RI, 2005.

[9] B. Manz, A. Coy, R. Dykstra, C.D. Eccles, M.W. Hunter, B.J. Parkinson, P.T. Callaghan, A mobile one-sided NMR sensor with a homogeneous magnetic field: the NMR-MOLE, J. Magn. Reson. 183 (2006) 25–31.

[10] A.E. Marble, I.V. Mastikhin, B.G. Colpitts, B.J. Balcom, A constant gradient unilateral magnet for near-surface MRI profiling, J. Magn. Reson. 183 (2006) 228–234.

[11] A.E. Marble, I.V. Mastikhin, B.G. Colpitts, B.J. Balcom, A compact permanent magnet array with a remote homogeneous field, J. Magn. Reson. 186 (2007) 100–104.

[12] C.L. Bray, J.P. Hornak, Unilateral MRI using a rastered projection, J. Magn. Reson. 188 (2007) 151–159.

[13] A. Marko, B. Wolter, W. Arnold, Application of a portable nuclear magnetic resonance surface probe to porous media, J. Magn. Reson. 185 (2007) 19–27.

[14] P.J. Mcdonald, P.S. Aptaker, J. Mitchell, M. Mulheron, A unilateral NMR magnet for sub-structure analysis in the built environment: the surface GARField, J. Magn. Reson. 185 (2007) 1–11.

[15] A. Guthausen, G. Zimmer, P. Blümler, B. Blümich, Analysis of Polymer Materials by Surface NMR via the MOUSE, J. Magn. Reson. A 130 (1998) 1–7.

[16] H. Kuhn, M. Klein, A. Wiesmath, D.E. Demco, B. Blümich, J. Kelm, P.W. Gold, The NMR-MOUSE®: quality control of elastomers, Magn. Reson. Imaging 19 (2001) 497–499.

[17] B. Blümich, S. Anferova, S. Sharma, A.L. Segre, C. Federici, Degradation of historical paper: nondestructive analysis by the NMR-MOUSE, J. Magn. Reson. 161 (2003) 204–209.

[18] H.T. Pedersen, S. Ablett, D.R. Martin, M.J.D. Mallett, S.B. Engelsen, Application of the NMR-MOUSE to food emulsions, J. Magn. Reson. 165 (2003) 49–58.

[19] S.K. Brady, M.S. Conradi, C.M. Vaccaro, NMR detection of thermal damage in carbon fiber reinforced epoxy resins, J. Magn. Reson. 172 (2005) 342–345.

[20] J. Perlo, F. Casanova, B. Blümich, Velocity imaging by ex situ NMR, J. Magn. Reson. 173 (2005) 254–258.

[21] F. Casanova, J. Perlo, B. Blümich, Velocity distributions remotely measured with a single-sided NMR sensor, J. Magn. Reson. 171 (2004) 124–130.

[22] C.A. Meriles, D. Sakellariou, H. Heise, A.J. Moulé, A. Pines, Approach to high-resolution ex situ NMR spectroscopy, Science 293 (2001) 82–85.

[23] D. Topgaard, R.W. Martin, D. Sakellariou, C.A. Meriles, A. Pines, "Shim pulses" for NMR spectroscopy and imaging, Proc. Natl. Acad. Sci. 101 (2004) 17576–17581.

[24] J. Perlo, V. Demas, F. Casanova, C.A. Meriles, J.R. Reimer, A. Pines, B. Blümich, High-resolution NMR spectroscopy with a portable single-sided sensor, Science 308 (2005) 1279.

[25] J. Perlo, F. Casanova, B. Blümich, Ex situ NMR in highly homogeneous fields: 1H spectroscopy, Science 315 (2005) 1110–1112.

[26] K. Halbach, Design of permanent multipole magnets with oriented rare earth cobalt material, Nucl. Instr. Meth. 169 (1980) 1–10.

[27] G. Moresi, R. Magin, Miniature permanent magnet for table-top NMR, Concepts Magn. Reson. B 19 (2003) 35–43.

[28] H. Raich, P. Blümler, Design and construction of a dipolar Halbach array with a homogeneous field from identical bar magnets: NMR Mandhalas, Concepts Magn. Reson. B 23 (2004) 16–25.

[29] B.P. Hills, K.M. Wright, D.G. Gillies, A low-field, low-cost Halbach magnet array for open-access NMR, J. Magn. Reson. 175 (2005) 336–339.

[30] X. Zhang, V. Mahesh, D. Ng, R. Hubbard, A. Ailiani, B. O'Hare, A. Benesi, A. Webb, Design, construction and NMR testing of a 1 tesla Halbach Permanent Magnet for Magnetic Resonance, in: COMSOL Multiphysics Conference, Boston, MA, 2005.

[31] K.R. Minard, R.A. Wind, Picoliter 1H NMR spectroscopy, J. Magn. Reson. 154 (2002) 336–343.

[32] V. Demas, J. Herberg, V. Malba, A. Bernhardt, L. Evans, C. Harvey, S.C. Chinn, R.S. Maxwell, J. Reimer, Portable, low-cost NMR with laser-lathe lithography produced microcoils, J. Magn. Reson. 189 (2007) 121–129.

[33] B. Manz, M. Benecke, F. Volke, Magnetanordnung zur Erzeugung eines NMR-fähigen homogenen Permanentmagnetfeldes, DE Patent No F107R380PCT (pending).

[34] J.D. Jackson, Classical Electrodynamics, John Wiley & Sons, New York, 1962.
[35] W.H. Press, B.P. Flannery, S.A. Teukolsky, W.T. Vetterling, Numerical recipes in C: the art of scientific computing, Cambridge University Press, Cambridge (UK), 1992.
[36] J. Murphy-Boesch, A.P. Koretsky, An in vivo NMR probe circuit for improved sensitivity, J. Magn. Reson. 54 (1983) 526–532.
[37] T. Haishi, T. Uematsu, Y. Matsuda, K. Kose, Development of a 1.0 T MR microscope using a Nd–Fe–B permanent magnet, Magn. Reson. Imaging 19 (2001) 875–880.